Tetragonal tungsten oxide nanobelts synthesized by chemical vapor deposition

Wei Wu [a,b], Qingkai Yu [a,b,*], Jie Lian [c], Jiming Bao [b], Zhihong Liu [b], Shin-Shem Pei [a,b]

[a] Center for Advanced Materials, University of Houston, Houston, TX 77204, USA
[b] Electrical and Computer Engineering, University of Houston, Houston, TX 77204, USA
[c] Mechanical, Aerospace, and Nuclear Engineering, Rensselaer Polytechnic Institute, Troy, NY 12180, USA

ARTICLE INFO

ABSTRACT

Tungsten trioxide (WO_3) nanobelts in tetragonal structure were grown on Si substrates by a hot-wall chemical vapor deposition (CVD) method without using catalysts. The products were characterized by scanning electron microscopy (SEM), X-ray diffraction (XRD), transmission electron microscopy (TEM), Raman spectroscopy, and photoluminescence (PL) spectrum. The width of the nanobelts is in the range of 50–100 nm with width-to-thickness ratios of 5–10 and lengths of up to tens of micrometers. These nanobelts grew along the [0 0 1] direction and can be identified as the tetragonal WO_3 structures. Raman and PL measurements indicate the high quality of the nanobelts. The vapor–solid growth mechanism could be applicable in our experiment.

1. Introduction

The nanowires and nanobelts of semiconductor oxides have attracted much attention due to their potential in nanoelectronics and optoelectronics [1–5]. With salient electrochromic, optochromic, gaschromic, and catalytic properties, tungsten oxides (WO_x) are of great interest, being promising in applications such as flat panel displays, 'smart windows', semiconductor gas sensors, and photocatalysts [6–9]. In the past few years, diverse forms of WO_x nanowires have been synthesized including monoclinic $W_{18}O_{49}$ nanowires [10,11], orthorhombic W_3O_8 nanowires [12], quasi-1D W_5O_{14} crystals [13], two-dimensional tetragonal $WO_{2.9}$ nanowire networks [14], monoclinic WO_3 nanowires [11,15], and cubic-structured WO_3 nanowires [16]. However, WO_x nanobelts are less observed and studied [17,18], although many other semiconductor oxides were vastly synthesized in nanobelts form such as ZnO, SnO_2, In_2O_3, CdO, Ga_2O_3, and PbO_2 [19].

In this paper, we report a catalyst-free growth of tetragonal WO_3 nanobelts on Si substrates in a simple way using a vapor–solid (VS) growth mechanism. The ratio of width to thickness of the nanobelts is 5–10 and the length can be up to tens of microns. WO_3 has a perovskite-like structure based on the corner sharing of WO_6 octahedra. With respect to the ideal cubic perovskite type, the symmetry of WO_3 is lowered resulting from two distortions:

tilting of WO_6 octahedra and displacement of tungsten from the center of its octahedron [20]. Pure WO_3 crystals exhibit at least five polymorphs in the temperature range varying from absolute zero to melting point at 1700 K, according to the following sequence monoclinic (ε phase)→triclinic (δ phase)→monoclinic (γ phase)→orthorhombic (β phase)→tetragonal (α phase). At room temperature a monoclinic (γ phase) and a triclinic modification are stable (or metastable) [21]. However, very limited results have been reported on the presence of high temperature phase of WO_3 in the tetragonal structure at room temperature [22,23].

2. Experimental

The WO_3 nanobelts were prepared by thermal evaporation of $WO_{2.9}$ powder (0.1 g, Alfa, 99.99% in purity) in a conventional horizontal tube furnace. The furnace was 30 cm long and has a zone of 10 cm of uniform temperature. The $WO_{2.9}$ powder was deposited into an alumina boat and placed in the uniform-temperature zone of the tube furnace, which acted as the source material. A silicon (1 0 0) wafer was placed in the low temperature zone, ∼8 cm downstream from the source, and acted as the substrate for WO_3 collection. The furnace system was first evacuated down to about ∼70 mTorr. Then, high purity H_2 (10 sccm, standard cubic centimeter per minute) was introduced, and system pressure was kept at ∼300 mTorr in the following processes. The furnace was heated to reach 900 °C at a heating

* Corresponding author at: Center for Advanced Materials, University of Houston, Houston, TX 77204, USA. Tel.: +1 713 7433621; fax: +1 713 7437724.
E-mail address: qyu2@uh.edu (Q. Yu).

rate of 20 °C·min⁻¹. The temperature of the substrate was increased concurrently to 500 °C. After 1.5 h, the temperature decreased gradually to room temperature. WO₃ nanobelts were finally produced on the substrate.

The as-synthesized product was examined initially using a LEO 1525 SEM. Further structural characterization of the detailed 1D nanostructures was carried out with XRD and high resolution TEM (HRTEM). Selected area electron diffraction (SAED) and energy dispersive X-ray spectroscopy (EDS) investigations were also conducted during the TEM experiments. Raman and PL spectra were performed using a Triax 550 single grating spectrometer equipped with a liquid nitrogen-cooled CCD detector. A 532 nm solid state laser was used for Raman measurement and a 325 nm He-Cd laser was used as an excitation source for photoluminescence.

3. Results and discussion

Fig. 1 shows SEM images at different magnifications and locations for a typical sample of the WO₃ nanobelts grown on the Si substrate. It can be seen that the product consists of a pure wire-like structure with a high density in a large scale (Fig. 1a and b). The cross-section shape of the nanobelts can be observed with a proper angle at the ends of the nanobelts, as indicated by red arrows in Fig. 1c. The inset image in Fig. 1c shows the cross-section of a nanobelt perfectly along the direction of growth. The width of nanobelts is in the range of 50–100 nm with width-to-thickness ratios of 5–10 and lengths of up to tens of micrometers with aspect ratios higher than 100, which are quite uniform along their growth direction. On the side surface of Si substrates (Fig. 1d), the nanobelts grew on the surface with a rough vertical alignment. On the sample using the same method as that growing for the sample of Fig. 1 but without introducing H₂, no nanobelt is obtained.

The XRD spectrum of the WO₃ nanobelts is shown in Fig. 2. The diffraction peaks can be indexed to tetragonal WO₃ phase structure, with $a=b=7.390$ Å and $c=3.880$ Å (JCPDS 89-1287). The inset spectrum in Fig. 2 shows the peaks (4 2 2) and (1 1 3) close to each other around 75.5°, which is a unique feature of tetragonal WO₃. We noticed that the close peaks overlapping each other in XRD spectra can happen in mixed phases. To investigate the possibility that the featured double peaks around 75.5° come from the other mixed phases of WO₃ and WO₃₋ₓ, but not tetragonal WO₃, further analysis was carried out according to the XRD database of WO₃ and WO₃₋ₓ. We found that except the aforementioned tetragonal WO₃, only the monoclinic WO₃ structure (JCPDS 87-2375) has a peak at 75.459°, which can match one of the featured double peaks in our measured XRD spectrum. If our sample has monoclinic WO₃ phases, there would be other three peaks around 28.5° monoclinic phase. However, only one peak labeled as (1 1 1) of WO₃ in tetragonal structure is observed, as shown in Fig. 2. As per the analysis above, it is believed that our WO₃ nanobelts have a tetragonal phase. The broad peak observed between 15° and 35° (scale 2θ) is ascribed to the glass sample holder in XRD facility. The morphology and structure of the WO₃ nanobelts were further studied by TEM. Fig. 3a and b presents the bright field TEM images with the corresponding SAED pattern in the inset of Fig. 3b. The nanobelts are straight and have uniform sizes along their growth directions. In Fig. 3b, many stripes showing dark contrast along the growth directions can be observed. The SAED pattern (inset in Fig. 3b) can be indexed as tetragonal WO₃, consistent with the analysis of XRD. The growth direction of the tetragonal WO₃ nanobelts can be identified as [0 0 1] based on the bright field TEM image and corresponding SAED pattern. In addition to the diffraction set with
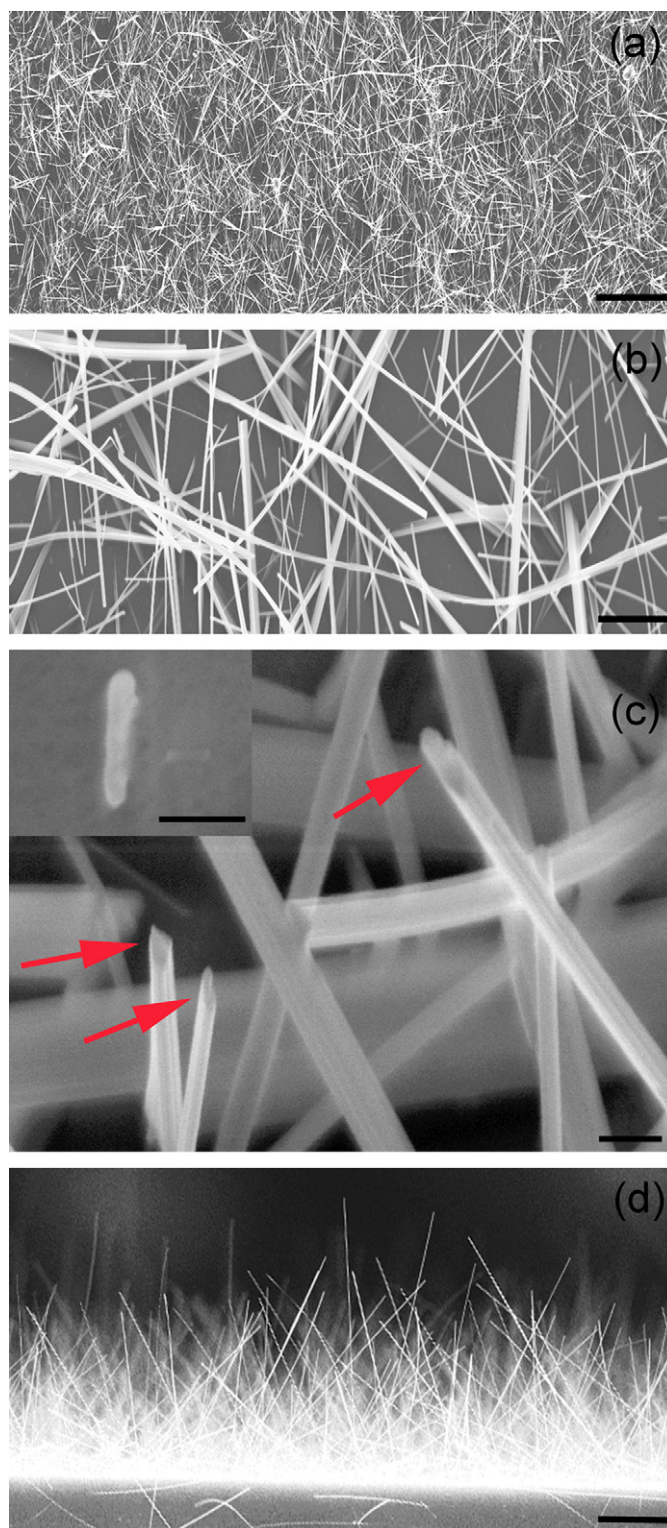

Fig. 1. SEM images of WO₃ nanobelts observed in different magnifications and angles. (a) Top view in low magnification. Scale bar is 20 μm. (b) Top view in medium magnification. Scale bar is 2 μm. (c) Top view in high magnification. Nanobelt shape can be identified from their end indicated by red arrows. Inset image shows the end of a nanobelt grown perpendicularly on a substrate (scale bar is 100 nm). (d) 90° side view of nanobelts grown on the side surface of Si substrates. Scale bar is 5 μm.

bright contrast resulting from the tetragonal WO₃, satellite diffractions showing weak contrasts were also identified, which can be attributed to the diffraction of strip features in bright field
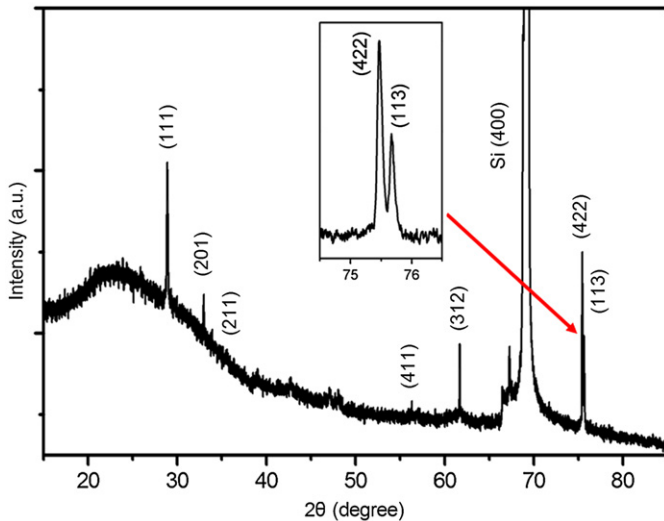
Fig. 2. XRD spectrum of as-synthesis WO_3 nanobelts on a Si substrate. The inset spectrum shows the peaks (4 2 2) and (1 1 3) close to each other around 75.5°, which is a feature of tetragonal WO_3.
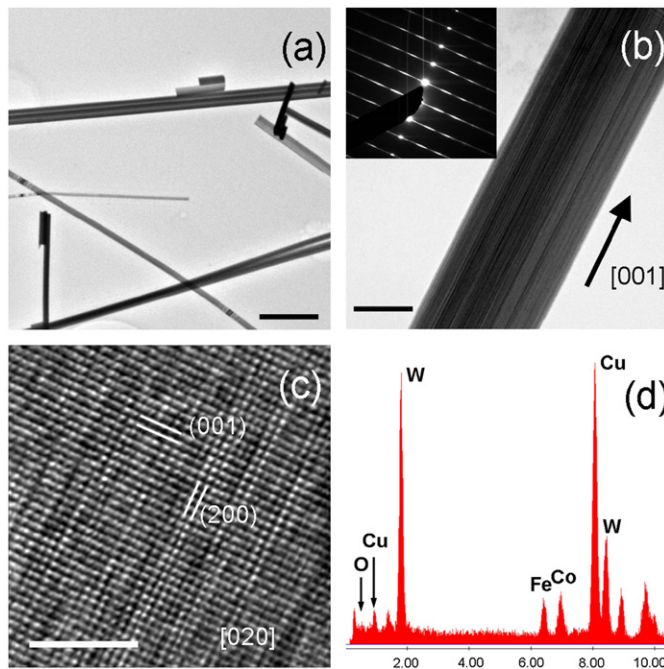

Fig. 3. TEM images of WO_3 nanobelts. (a) Low magnification image. Scale bar is 1 μm. (b) High magnification image with SAED pattern shown in inset image. Scale bar is 50 nm. SAED pattern (inset in Fig. 3b) can be indexed as tetragonal WO_3 and the growth direction of the tetragonal WO_3 nanobelts can be identified as [0 0 1]. (c) HRTEM image shows the lattice spacing are 0.388 and 0.739 nm, respectively. Scale bar is 5 nm. (d) EDX spectrum indicates the W and O elements. Cu signal is from TEM grid and Co and Fe signals are from contamination in TEM chamber.

TEM image (Fig. 3b). This contrast variation is also evident in the HRTEM image (Fig. 3c), and the lattice spacing can be measured to be 0.388 and 0.739 nm, respectively, as shown in Fig. 3c, consistent with the lattice space of tetragonal WO_3 (0 0 1) and (2 0 0) planes. The chemical composition of the WO_3 nanobelts was characterized by the EDS spectrum shown in Fig. 3d. It reveals that the nanobelts contain W and O only, in which Cu single was from the TEM grid and Co and Fe signals were from contaminants of the EDS detector, respectively.

The appearance of satellite diffraction and dark strips in bright field TEM (BFTEM) image suggests that planar defects (e.g., stacking faults) may be induced in the crystalline lattice of the tetragonal WO_3 nanobelts during the growth process, leading to contrast variations. In addition, the incommensurate contrast variation (unequal space of satellite diffraction in SAED patterns) may be attributed to the chemical modulation as a result of long range ordering. Specifically, this incommensurately modulated structures are often observed in complex ceramics resulting from atomic ordering on crystallographically equivalent sites, leading to atomic positional displacements or from both structural distortions and fluctuations in composition [24]. Because of the relatively simple chemistry in WO_3 nanobelts, it may not be possible to induce a long range ordering as a result of chemical modulations. Instead, a structural distortion resulting from the tilting of WO_6 octahedra or the displacement of tungsten from the center of its octahedron may lead to the structural deviation from ideal pervoskite structure. Furthermore, defects such as oxygen vacancies may be ordered along the (2 0 0) plane of the tetragonal WO_3 nanobelts, resulting in contract variation in both SAED and BFTEM images. Because of the complex features of incommensurate modulation, diverse phase transitions and structural distortions in WO_3 polymorphs, it is difficult to understand what facts lead to the structural modulation observed in the tetragonal WO_3 nanobelts. Nevertheless, both SAED and HRTEM images show that the tetragonal WO_3 nanobelts are well crystallized.

Fig. 4 shows Raman spectrum of the WO_3 nanobelts at room temperature. Several clear features can be seen. The strong and sharp peak near 520 cm^{-1} and a broad peak near 950 cm^{-1} arise from silicon substrate. The spectrum is very close to, but not exactly identical with, any Raman spectra of tungsten oxides reported in the literature [25]. The high frequency lines at 810 and 682 cm^{-1} are believed to originate from stretching modes of O–W–O bonds, and the low frequency lines in the region of 100–400 cm^{-1} are due to their bending modes. The lines at 810, 326, and 133 cm^{-1} are relatively narrow in width, and have been observed in monoclinic WO_3 crystal at room temperature. The broader peaks at 256 and 682 cm^{-1} are red-shifted from the corresponding 272 and 716 cm^{-1} lines of monoclinic WO_3, but they are similar in width and position with lines observed in α-WO_3, which only exist at a high temperature above 900 K [26]. These
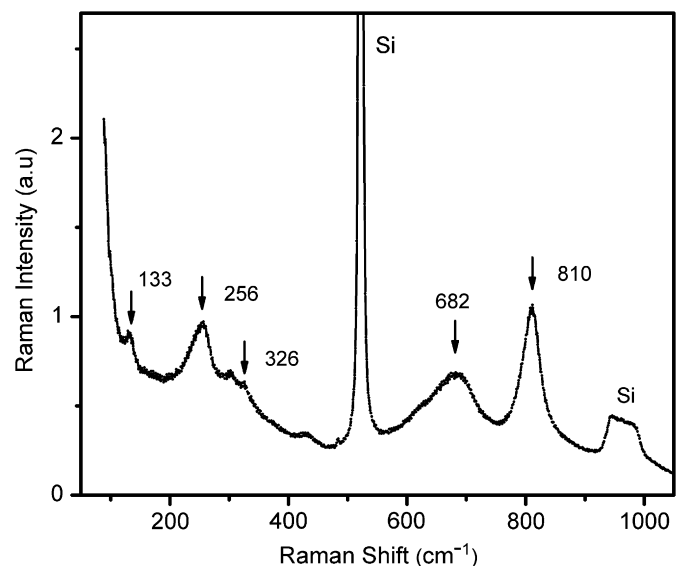

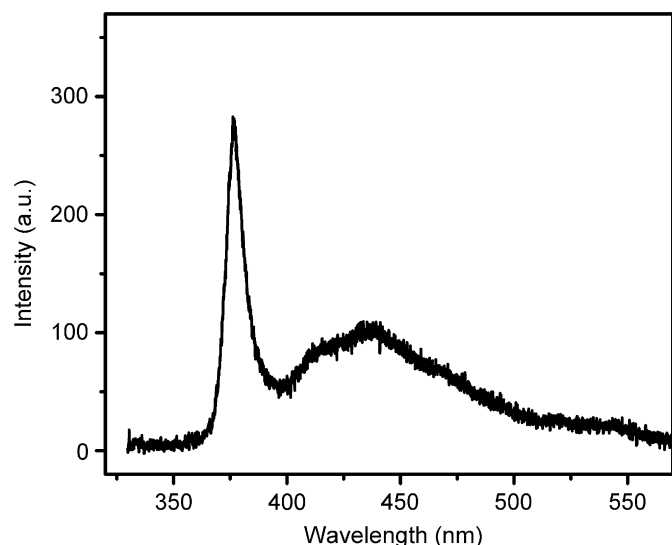**Fig. 4.** Raman spectrum of the WO_3 nanobelts at room temperature.

Fig. 5. PL spectrum of the WO$_3$ nanobelts, which reveals a weak ultraviolet emission at 376 nm.

unique Raman features indicate that the nanobelts possess a high quality crystalline structure that is different from those reported.

Fig. 5 shows room-temperature PL spectrum of the WO$_3$ nanobelts, revealing a weak ultraviolet emission at 376 nm. The broad feature centered at 430 nm comes from native oxide of substrate silicon. This narrow UV PL hasn't been reported in any other tungsten oxides. UV PL peaks at 351 and 361 nm from W$_{18}$O$_{49}$ nanowires were obtained by Hong et al. [10]. Luo et al. [27] also reported a strong luminescence peak at 395 nm from WO$_{3-x}$ nanowire networks, and they attributed this emission to the state of oxygen vacancies in the nanowire network. The narrow line width and weakness of this UV emission indicate a high quality of crystal structure and nature of indirect bandgap of our nanobelts.

Based on the observations above, we propose a possible growth mechanism for the formation of WO$_3$ nanobelts. In general, two mechanisms, vapor–liquid–solid (VLS) [28] and vapor–solid (VS) [29,30], have been most commonly used to explain the growth of 1D nanostructures. In our study, no catalysts were used and none of the nanobelts was terminated in particles, so the VS mechanism is likely responsible for the growth of WO$_3$ nanobelts in our experiment. In a typical VS process, the constituents of the nanobelts are evaporated from a solid source in a high temperature zone, and then delivered and deposited onto a substrate in a low temperature zone. To reveal the importance of H$_2$ for WO$_3$ nanobelts growth in our experiment, we have prepared samples using the same condition as previously described except that H$_2$ was not introduced. No nanobelts could be found by SEM after the treatment. It suggests that the existence of H$_2$ is necessary for nanobelt growth. We proposed the following growth model in the light of the existing VS mechanism. As the temperature gradually increased to, and at the final temperature of 900 °C, volatile tungsten oxide was formed as WO$_3 \cdot$H$_2$O vapor with the presence of H$_2$ and O$_2$ by leakage under vacuum. The WO$_3 \cdot$H$_2$O vapor was transported and then decomposed and condensed into WO$_3$ clusters in a nucleation step on the substrate in the low temperature region. In general, the growth of nanobelts is kinetically controlled owing to the different diffusion capabilities on different crystallographic planes. However, for WO$_3$ nanobelts, the thickness and width directions are crystallographically equivalent and kinetics cannot explain this phenomenon. In our research, we found that the WO$_3$

nanobelts are not freestanding, but took root on the Si (1 0 0) substrate. It is expected that the nucleation process of WO$_3$ nanobelts was confined by the substrate and the diffusion and impingement behaviors of WO$_3$ molecules are different in different crystallographic directions of Si substrate. The nucleus of WO$_3$ nanoclusters can form in a rectangular shape on Si substrate and nanobelts can grow from the rectangular nucleus.

4. Conclusions

In summary, high density, uniform Tungsten trioxide nanobelts were synthesized on Si substrate in a large scale by the CVD method without any catalyst. The width of the nanobelts is in the range of 50–100 nm with width-to-thickness ratios of 5–10 and lengths of up to tens of micrometers. These nanobelts grew along the [0 0 1] direction in the tetragonal WO$_3$ structures. Raman and PL measurements indicate the high quality of the nanobelts. A vapor–solid growth model was proposed to illustrate the formation of tungsten trioxide nanobelts in our experiment. The influence of H$_2$ is also discussed.

Acknowledgment

References

[1] Z.L. Wang, Adv. Mater. 15 (2003) 432.
[2] G. Sberveglieri, Sensors Actuators B 23 (1995) 103.
[3] M.H. Huang, S. Mao, H. Feick, H.Q. Yan, Y.Y. Wu, H. King, E. Weber, R. Russo, P.D. Yang, Science 292 (2001) 1897.
[4] G. Du, Q. Chen, R. Che, Z. Yuan, L. Peng, Appl. Phys. Lett. 79 (2001) 3702.
[5] H. Cheng, Y. Chen, H. Lin, C. Mou, Appl. Phys. Lett. 78 (2001) 3791.
[6] C. Sanrato, M. Odziemkowski, M. Ulmann, J. Augustynski, J. Am. Chem. Soc. 123 (2001) 10639.
[7] S.H. Baeck, K.S. Choi, T.F. Jaramillo, G.D. Stucky, Adv. Mater. 15 (2003) 1269.
[8] H. Meixner, J. Gerblinger, U. Lampe, M. Fleischer, Sens. Actuators B 23 (1995) 119.
[9] J.L. Solis, S. Saukko, L. Kish, C.G. Granqvist, V. Lantto, Thin Solid Films 391 (2001) 255.
[10] K. Hong, M.H. Xie, R. Hu, H.S. Wu, Appl. Phys. Lett. 90 (2007) 173121.
[11] Y. Zhang, Y. Chen, H. Liu, Y. Zhou, R. Li, M. Cai, X. Sun, J. Phys. Chem. C 113 (2009) 1746.
[12] R. Hu, H. Wu, K. Hong, J. Cryst. Growth 306 (2007) 395.
[13] M. Remskar, J. Kovac, M. Virsek, M. Mrak, A. Jesih, A. Seabaugh, Adv. Funct. Mater. 17 (2007) 1974.
[14] Y.M. Zhao, Y.H. Li, I. Ahmad, D.G. McCartney, Y.Q. Zhu, W.B. Hu, Appl. Phys. Lett. 89 (2006) 133116.
[15] Y. Baek, K. Yong, J. Phys. Chem. C 111 (2007) 1213.
[16] J. Zhou, Y. Ding, S.Z. Deng, L. Gong, N.S. Xu, Z.L. Wang, Adv. Mater. 17 (2005) 2107.
[17] Y.B. Li, Y. Bando, D. Golberg, K. Kurashima, Chem. Phys. Lett. 367 (2003) 214.
[18] H. Wang, X. Quan, Y. Zhang, S. Chen, Nanotechnology 19 (2008) 065704.
[19] Z.L. Wang, Z.W. Pan, Int. J. Nanosci. 1 (2002) 41.
[20] P.M. Woodward, A.W. Sleight, T. Vogt, J. Solid State Chem. 131 (1996) 9.
[21] E. Salje, K. Viswanathan, Acta Crystallogr. A31 (1975) 356.
[22] A. Aird, M.C. Domeneghetti, F. Mozzi, V. Tazzoli, E.K.H. Salje, J. Phys.: Condens. Matter 10 (1998) L569.
[23] K.P. Locherer, I.P. Swainson, E.K.H. Salje, J. Phys.: Condens. Matter 11 (1999) 4143.
[24] P. Buseck, J. Cowley, E. Leroy, High Resolution Transmission Electron Microscopy and Associates Techniques, Oxford Sciences, pp. 340–342.
[25] D.Y. Lu, J. Chen, H.J. Chen, L. Gong, S.Z. Deng, N.S. Xu, Y.L. Liu, Appl. Phys. Lett. 90 (2007) 041919.
[26] M. Boulova, G. Lucazeau, J. Solid State Chem. 167 (2002) 425.
[27] J.Y. Luo, F.L. Zhao, L. Gong, H.J. Chen, J. Zhou, Z.L. Li, S.Z. Deng, N.S. Xu, Appl. Phys. Lett. 91 (2007) 093124.
[28] R.S. Wagner, W.C. Ellis, Appl. Phys. Lett. 4 (1964) 89.
[29] I. Matsubara, H. Kageyama, H. Tanigawa, T. Ogura, H. Yamashita, T. Kawai, Jpn. J. Appl. Phys. 28 (1989) L1121.
[30] R. Funahashi, I. Mastsubara, M. Shikano, Chem. Mater. 13 (2001) 4473.